ISSN 1070-3284, Russian Journal of Coordination Chemistry, 2022, Vol. 48, No. 12, pp. 846–858. © Pleiades Publishing, Ltd., 2022.

The Effect of the Ancillary Ligand on Optical and Redox Properties of Cyclometalated Iridium(III) 2,5-Diphenyloxazole Complexes

A. Yu. Zakharov[a], I. V. Kovalenko[a, b], E. A. Meshcheriakova[a, b], E. V. Nykhrikova[a, b], A. O. Zharova[a, b], M. A. Kiseleva[a, b], P. Kalle[a], E. V. Tekshina[a], S. A. Kozyukhin[a], V. V. Emets[c], and S. I. Bezzubov[a, *]

[a] *Kurnakov Institute of General and Inorganic Chemistry, Russian Academy of Sciences, Moscow, 119991 Russia*

[b] *Department of Chemistry, Moscow State University, Moscow, 119991 Russia*

[c] *Frumkin Institute of Physical Chemistry and Electrochemistry, Russian Academy of Sciences, Moscow, 119071 Russia*

**e-mail: stas.bezzubov@gmail.com*

Received September 6, 2022; revised September 9, 2022; accepted September 10, 2022

Abstract—Two series of bis-2,5-diphenyloxazolato cyclometalated iridium(III) complexes with substituted 2,2'-bipyridine or dipyridophenazine as the ancillary ligand have been prepared and characterized by X-ray structural analysis, ^{1}H NMR, and high resolution mass spectrometry. Bipyridine-based complexes exhibited bright emission in the yellow-orange region in solution, whereas their dipyridophenazine analogues demonstrated low quantum yields in the same spectral area. Varying the substituents in the ancillary ligand (CH_3, H, COOH) caused noticeable shifts of the long-wavelength absorption bands retaining the redox potentials of the complexes practically unchanged. Crystallization of the complexes with iodine species gave interesting salts containing infinite polyiodide chains forming intermolecular contacts with the π-system of the ligands. Complexes bearing "anchoring" COOH-groups were used in sensitization of titania photoanodes followed by their study under the AM 1.5 G condition.

Keywords: iridium, oxazole, X-ray crystallography, dye-sensitized solar cell, UV-vis spectroscopy, polyiodide

DOI: 10.1134/S1070328422700051

INTRODUCTION

Cyclometalated iridium(III) complexes are very attractive as bright emitters for optoelectronics due to their unique photophysical properties along with high thermodynamic and kinetic stability [1, 2]. These compounds are of particular interest because their emission colour can be varied over the whole visible spectral range by changing the electron-donating/withdrawing ability of substituents in cyclometalated (C^N) ligands [3]. Still, this strategy to tune the emission energy of the complexes does not allow to simultaneously retain stability and high quantum yields in the "blue" and near-infrared ranges. So, numerous ancillary ligands have been examined in bis-cyclometalated iridium(III) complexes and several stable and efficient "blue" or near-infrared emitting complexes have been obtained [4–7].

Emission and photosensitization are closely related processes because they both utilize (although in different ways) the deactivation of the triplet excited state of iridium(III) complexes [8]. In line with this, some structure-property correlations obtained from studies of iridium(III) phosphors are used in design of iridium-based dyes for solar cell application [1]. Indeed, the increase in the electron-donating ability of cyclometalated ligands usually leads to a bathochromic shift of the absorption maxima [9–11] while the extension of their conjugated π-system enhances molar absorptivity of iridium(III) complexes [12–14]. Still, the above simple and common approaches do not represent a panacea for the challenges facing the creation of an ideal iridium(III) photosensitizer. There have been several reports on iridium(III) complexes bearing strong NMe_2 or NPh_2 π-donors which demonstrated poor light-harvesting properties in the visible spectral range, very low photoluminescence quantum yields and irreversible redox behavior [11, 15–17].

Decrease in the contribution of iridium d-orbitals to the highest occupied molecular orbital (HOMO) of the complexes caused by a very strong π-donating ability of the substituents diminished the probability of the metal-to-ligand charge transfer (MLCT) that negatively affected both the intensity of long-wavelength absorption bands and the radiative decay rate of the complexes [18]. Furthermore, the oxidation of the iridium(III) dyes accompanied by removal an electron from the HOMO can, hence, be better described as the irreversible oxidation of the negatively charged cyclometalated ligands rather than the reversible oxidation of the iridium center [19]. The extension of the conju-

gated π-system of cyclometalated ligands can cause a destabilization of the octahedral geometry around the iridium(III) ion because of the steric hindrance induced by the bulky ligands [20, 21], so the corresponding iridium(III) dyes can scarcely work long-term in solar cells.

As in the case of iridium(III) phosphors, the change of the ancillary ligand may be a valid approach to improve the characteristics of iridium(III) dyes though ligands bearing "anchoring" acid groups can only be selected. Still, 4,4'-dicarboxy-2,2'-bipyridine (H_2dcbpy) remains the most popular "anchoring" ligand in iridium(III) complexes (the same is true for many other metals) for application in dye-sensitized solar cells [1, 22–26] and less attention has been paid to the exploration of other ancillary ligands in this role [27, 28].

Studies of 2-arylbenzimidazole and aryl-triazole iridium(III) complexes with various ancillary ligands identified several factors affecting nuclearity, structure, photophysical properties as well as solubility of the complexes (Scheme 1) [17, 29–31]. In continuation of this work, we synthesized iridium(III) complexes with 2,5-diphenyl-1,3-oxazole which is structurally similar to 2-arylbenzimidazoles but is much less investigated as the cyclometalated ligand. Some derivatives of 2,2'-bipyridine or dipyrido[3,2-a:2',3'-c]phenazine as ancillary ligands were used to study the influence of the size of the ancillary ligand (particularly, determining the distance between the metal center and the semiconductor surface which in turn can affect the charge recombination in solar cells [32]) and its electronic properties (tuned by the substituents) on optical and redox characteristics of the resulting complexes.

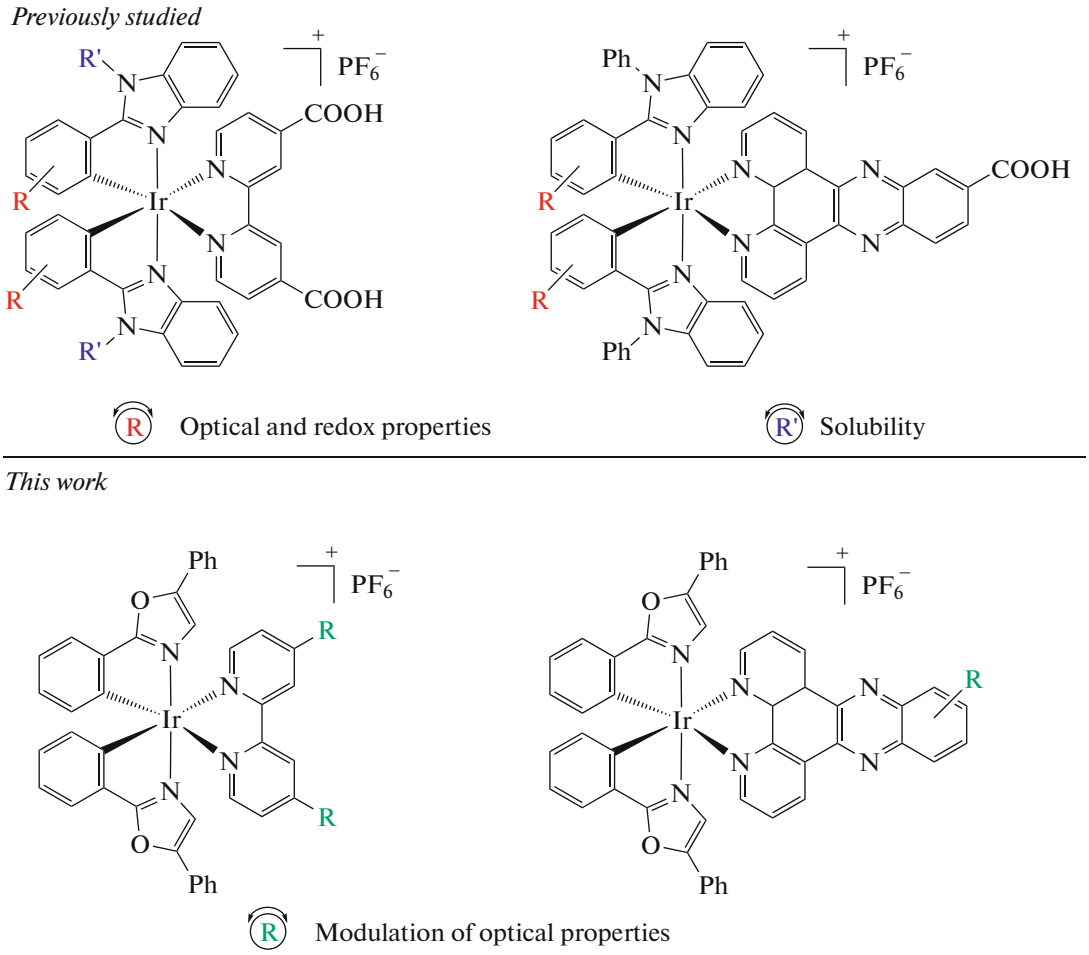

Scheme 1. The previously established effect of aryl- (R) and *N*- (R^I) substituents on optical and redox properties as well as solubility of cyclometalated iridium(III) complexes (top) and the opportunity to finely tune the photophysical characteristics of the complexes by changing substituents in the ancillary *N*-donor ligands revealed in this work (bottom).

RESULTS AND DISCUSSION

Synthesis and Structure

Bis-2,5-diphenyloxazolato cyclometalated chloro-bridged iridium(III) dimer was prepared in high yield (86%) and characterized by ^{1}H NMR. Cleavage of the dimer by addition of the ancillary ligand followed by replacement of the chloride anion with electrochemically inert hexafluorophosphate gave heteroleptic cationic complexes **1**–**6** (Scheme 2) which were characterized by ^{1}H NMR, high-resolution mass spectrometry (Figs. S1–S13) and single-crystal X-ray analysis (Table S1).

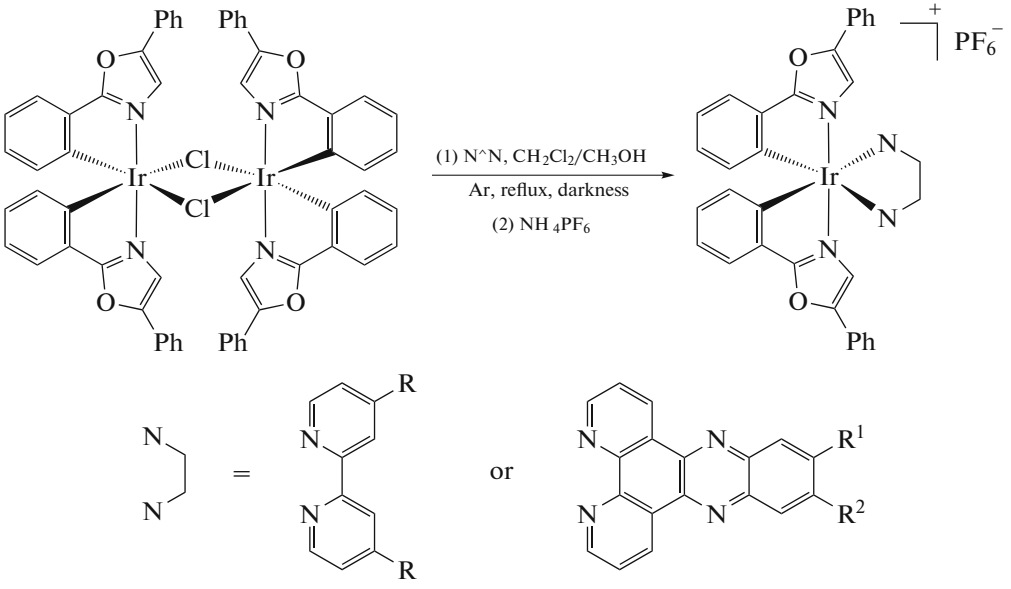

R	H	CH_3	COOH	R^1, R^2	H, H	CH_3, CH_3	H, COOH
Complexes	**1**	**2**	**3**		**4**	**5**	**6**

Scheme 2. Synthesis of complexes **1**–**6** (N^N—ancillary ligand).

In the complexes, the ligands form a common distorted octahedral geometry around the metal ion with *trans*-N_1,N_2 coordination of the cyclometalated ligands while the N_3, N_4 donor atoms of the ancillary ligands lie opposite to the metalated carbon atoms (Fig. 1). The Ir–C and Ir–N_1(N_2) interatomic distances are within the range from 2.029(7) to 2.044(9) Å and 2.023(6) to 2.049(7) Å, respectively, whereas the Ir–N_3(N_4) bonds are slightly longer (2.115(6) to 2.148(4) Å) because of *trans*-effect of the stronger Ir–C bonds (Table S2).

While the aromatic parts of 2,5-diphenyloxazoles forming metallacycles are almost flat the 5-phenyl ring of these ligands is rotated to a relatively small angle (<20°) with the oxazole ring. The tendency for this phenyl ring to assume an almost coplanar conformation (which can also be seen from published structures containing 2,5-diphenyloxazole) seems to result from resonance interaction between the 5-phenyl ring and the cyclometalated moiety of the ligand.

In crystals, bpy-based cationic complexes **1** and **2** are combined by C–H···π interactions forming the 3D packing containing layers or cavities filled by disordered PF_6^- anions and/or solvent CH_2Cl_2. In the crystal of **5**, the complex cations are held together by C–H···π contacts giving a very loose packing with two sets of large channels passing along the *b* axis, one of which contains rotationally disordered PF_6^- anions while the other is filled by highly disordered solvent CH_2Cl_2. In the crystal of **6**, moderate C–H (oxazole)···O (carboxyl) hydrogen bonds and weak π···π stacking between the phenazine moieties assemble cations in centrosymmetric pairs interacting with each other through C–H···π contacts. The carboxy-groups form short H-bonded chains including two solvent methanol molecules and one PF_6^- anion.

Study of the dye–mediator interactions in dye-sensitized solar cells is particularly important for understanding the charge transfer mechanism in the cells that can be useful for eliminating "parasitic" recombination processes [33–36]. Dye molecules can react with various iodine species (I_2, I^-, I_3^- or longer polyiodides) on the TiO_2 surface that results in quenching of

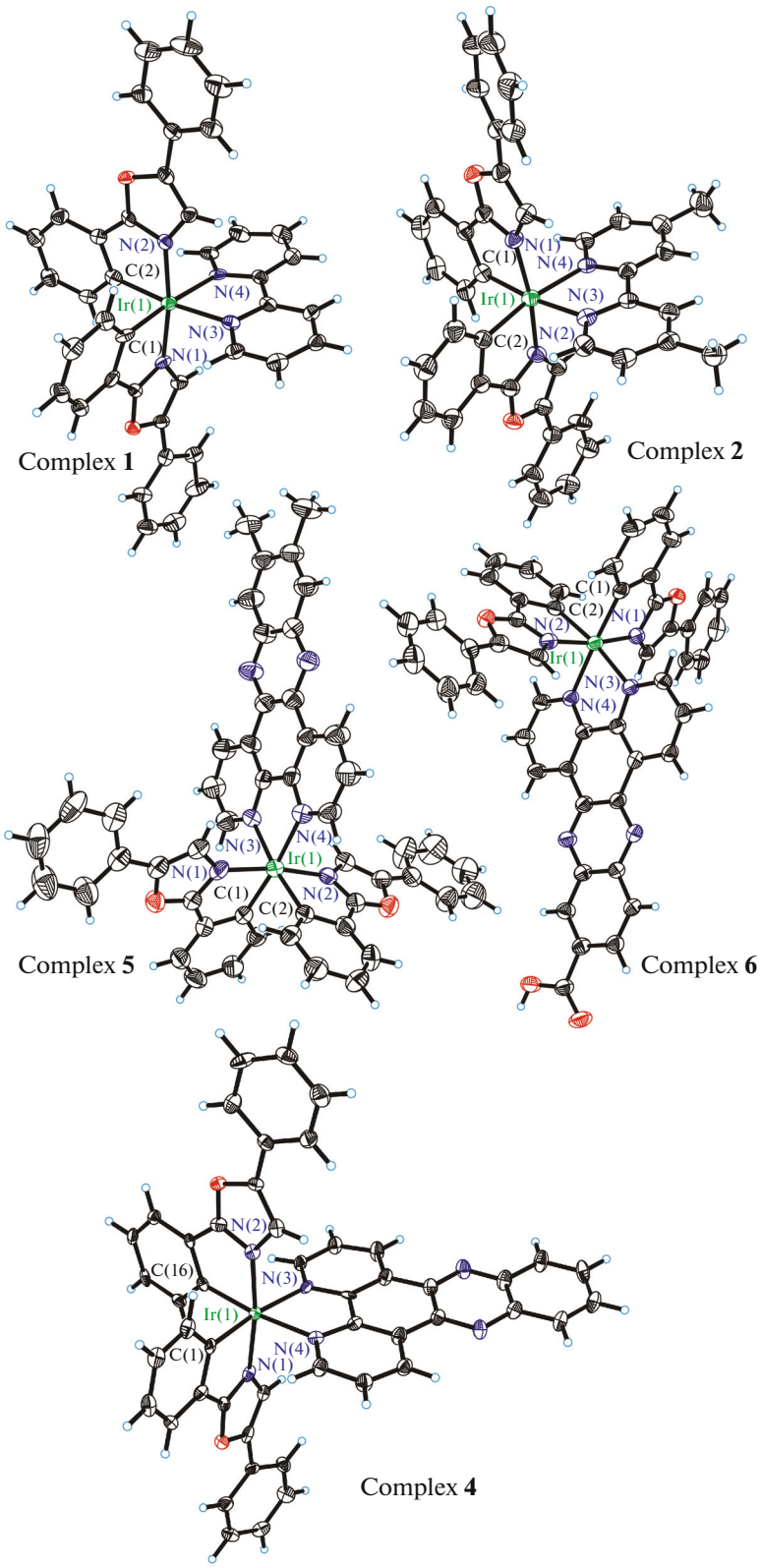

Fig. 1. Molecular structures of complexes **1**, **2**, **4**, **5**, and **6**. Displacement ellipsoids are shown at the 50% probability level. Counterions (PF_6^- or polyiodides) are not presented.

Table 1. Redox and optical characteristics of complexes **1**–**6**

Complex	$E_{1/2}$/V vs. Fc^+/Fc[a] redox		ΔE/V	E_{0-0}/eV	$E(Ir^{4+}/Ir^{3+*})$/V[b]	λ^{abs}/nm ($\varepsilon \times 10^{-3}/M^{-1}\,cm^{-1}$)[c]	λ^{em}/nm (PLQY/%)[d]
1	−1.81	0.97	2.78	2.48	−1.51	286 (56), 387 (13), 475_{sh} (1.1)	546, 585 (1.2)
2	−1.90	0.93	2.83	2.50	−1.57	286 (57), 387 (12), 475_{sh} (0.8)	594 (2.9)
3	−1.42	1.01	2.43	2.36	−1.35	286 (57), 389 (17), 475_{sh} (1.4)	616 (9.0)
4	−1.34, −2.03	0.98	2.32	2.45	−1.47	282 (72), 364 (18), 384 (16), 475_{sh} (1.0)	565 (0.3)
5	−1.46, −1.69	0.98	2.44	2.43	−1.45	290 (71), 375 (20), 389 (20), 475_{sh} (0.5)	569 (0.4)
6	−1.18	1.02	2.20	2.40	−1.38	285 (70), 370 (17), 386 (17), 475_{sh} (1.0)	571, 652 (0.5)

[a] Measured in Ar-saturated acetonitrile with 0.1 M (n-$Bu_4N)ClO_4$ at a scan rate of 100 mV/s. Ferrocene was used as an internal standard. $E_{Fc^+/Fc} = 0.64$ V. $\Delta E = E_{ox} - E_{red}$. Estimated error: ±20 mV for E_{ox} and E_{red}.

[b] Calculated from $E(Ir^{4+}/Ir^{3+*}) = E_{ox} - E_{0-0}$, where E_{0-0} was estimated from the onset of the emission spectrum at ca. 10% intensity.

[c] Measured in Ar-saturated CH_2Cl_2.

[d] λ_{ex} = 513 nm. PLQY—photoluminescence quantum yield relative to rhodamine 6G were measured in Ar-saturated CH_2Cl_2. Estimated error: ±0.1% for rel. PLQY. sh—shoulder.

the exited dye or recombination of the already injected electron [37–39]. These processes can scarcely be investigated in solution because of high mobility of the components while "freezing" the system in a single-crystal followed by thorough inspection of intermolecular interactions by X-ray analysis seems more reasonable [40]. In line with this, complexes **1, 2, 4, 5** were crystallized in the presence of an iodide/iodine mixture having the components ratio close to that in the common iodine-based electrolyte.

Single-crystals suitable for X-ray analysis were grown only for complexes **1** and **4**. Surprisingly, in the both cases we obtained crystals containing polyiodide chains stabilized by weak complex-iodine interactions.

In the first case, crystal $\mathbf{1}\cdot I_5^-$ contains slightly disordered V-shaped pentaiodide anions interacting with π-systems of cyclometalated and ancillary ligands (Fig. 2). Adjacent polyiodides are related to one another by a c axis and distant by 3.712(2) Å forming infinite chains passing along the c direction. In the second case, an asymmetric unit of crystal $\mathbf{4}\cdot I_3^-\cdot I_2$ comprises two halves of crystallographically independent symmetric triiodides each lying at inversion centers (Fig. 3). An iodine molecule holds these anions together (I···I contacts 3.242(2) and 3.536(3) Å) forming an infinite chain partially stabilized by intermolecular contacts between iodine atoms and π-system of the ancillary dipyridophenazine ligand and passing along the body diagonal of the cell.

Given the tendency of iodine to form halogen-bonded chains and especially in view of electrical conductivity of the latter [41–44], some authors stress the key role of polyiodide chains for the charge transfer in dye-sensitized solar cells [45–48]. The applied crystallization method allowed us growing good crystals for X-ray analysis, but, unfortunately, the crystals were too small for conductivity measurements. We tried to simulate the charge recombination process by irradiating the crystals under UV light (λ = 380 nm) according to [49], but the crystals did not retain crystallinity after this exposure. Still, the presented crystal data, although not exhaustive, demonstrate that in the dye-mediator system infinite polyiodide chains can be formed and additional studies of similar crystals may provide essential data for better understanding the charge transfer mechanism in dye-sensitized solar cells. With the reproducible method for growing dye-polyiodide crystals in hand, we are now working in two directions: to grow large crystals suitable for electrochemical measurements and to produce promising DSSCs with solid polyiodide electrolyte [50].

Optical and Redox Properties

In each short series **1**–**3** and **4**–**6** the change of substituents in the ancillary ligand causes just a little effect on absorption maxima of the complexes while altering noticeably their molar absorptivity (Fig. 4, Table 1). Complexes **3** and **6** having electron-withdrawing COOH-groups possess better light absorption in the visible spectral range which is likely due to larger dipole moments of their molecules. In contrast, the replacement of the ancillary ligand (2,2'-bipyridine to dipyridophenazine) results in significant enhancement of the absorption of the complexes in the UV ranges at 280–320 and 350–400 nm. The extended π-system of dppz and its derivatives favors the delocalization of the excited state increasing the probability of the corresponding $\pi \rightarrow \pi^*$ and MLCT electronic transitions.

All the complexes show photoluminescence in solution in the range from 550 to 650 nm with emission maxima and quantum yields depending on the ancillary ligand (Fig. 5, Table 1). In going from **1** to **3** the emission is noticeably shifted bathochromically while the quantum yield increases 7.5 times. In going from **4** to **6** the emission band is slightly red-shifted

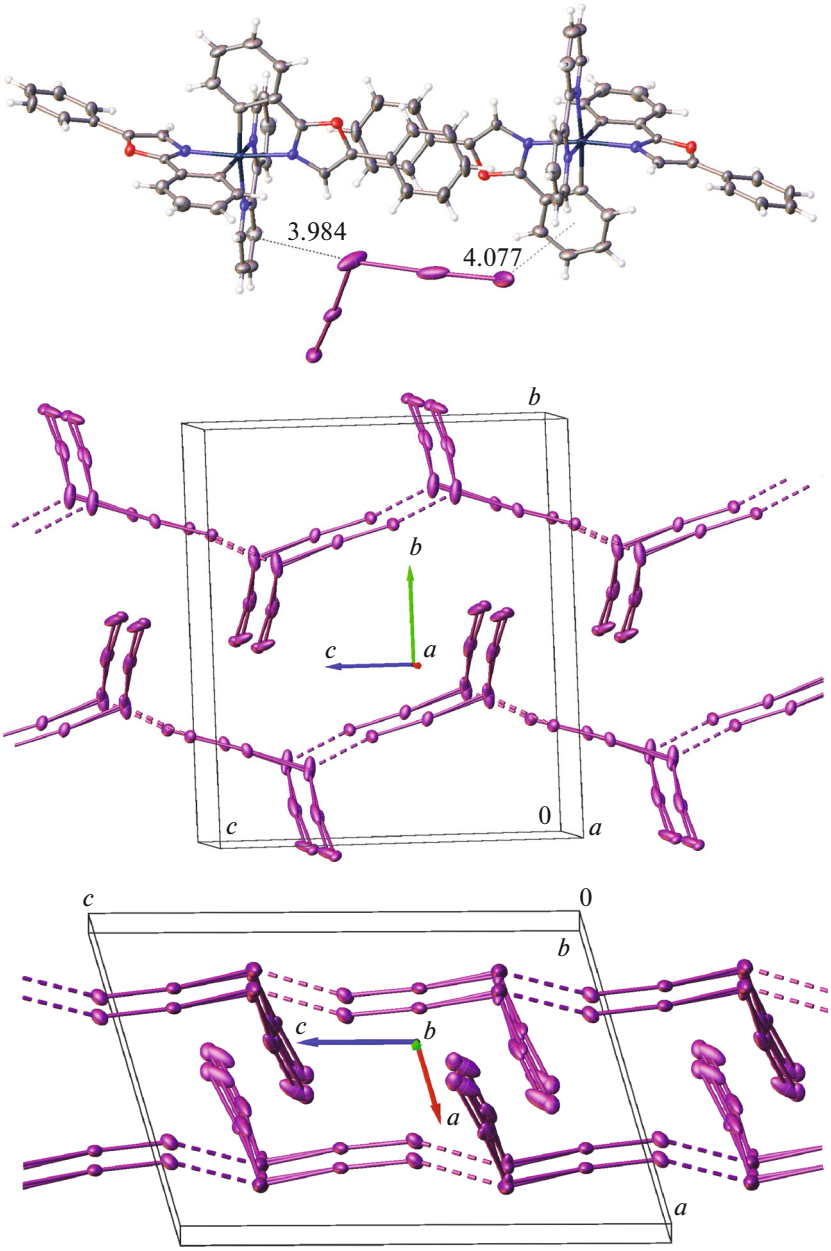

Fig. 2. Fragment of the crystal packing of **1**·I_5^- (top). Polyiodide chains in different views (middle, bottom). Distances are presented in Å. Displacement ellipsoids are shown at the 50% probability level.

while the quantum yield varies within the experimental error remaining less than 1%. Complexes **1**–**3** are about 10 times brighter emitters than **4**–**6** because the triplet excited state of the latter seems to delocalized over the extended conjugated π-system of the ancillary ligand and, hence, tends to deactivate non-radiatively.

All the complexes demonstrate reversible redox behavior with oxidation potentials being practically invariant to changes in the ancillary ligand and lying in the range 0.93–1.02 V vs. E(Fc^+/Fc) (Fig. S14). This suggests that the HOMOs of the complexes are mainly composed of iridium d-orbitals and π-orbitals of the cyclometalated ligand with a little contribution of the ancillary ligand orbitals.

Bipyridine-based complexes **1**–**3** show one reversible redox process at negative potentials with $E_{1/2}$ ranging from −1.90 to −1.42 V vs. E(Fc^+/Fc) upon the replacement of two methyl by two carboxy groups. This large positive shift of the reduction potential indicates that the added electron is delocalized throughout the ancillary ligand and, hence, the latter hosts the LUMOs of the complexes. Complexes **4**–**6** behave similarly to **1**–**3**, but more positive potentials are required to observe their reduction because dppz-

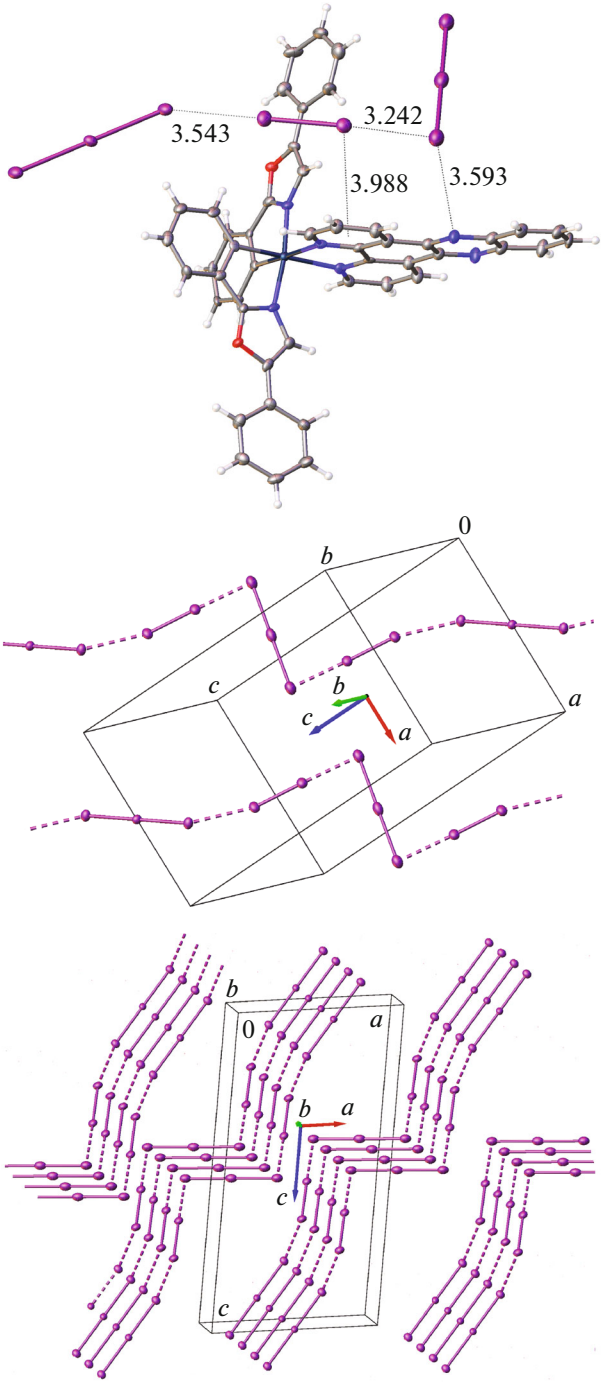

Fig. 3. Fragment of the crystal packing of $4 \cdot I_3^- \cdot I_2$ (top). Polyiodide chains in different views (middle, bottom). Distances are presented in Å. Displacement ellipsoids are shown at the 50% probability level.

based ancillary ligands seem to better delocalize the additional electron density than the derivatives of bpy. The CV curves of **4** and **5** contain one additional reduction wave at more negative potentials (−2.03 and −1.69 V vs. $E(Fc^+/Fc)$, respectively).

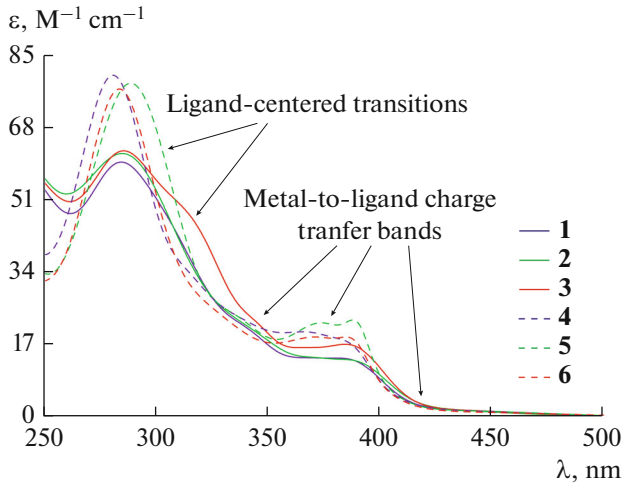

Fig. 4. UV-Vis spectra of **1**–**6** recorded in CH_2Cl_2 at 25°C with assignment of absorption bands according to [26].

DFT Calculations

An analysis of the composition and energy of molecular orbitals of complexes **1**–**6** (Table S3, Fig. S15) shows that the variation of the substituents in the ancillary ligand and even more considerable structural changes of the latter slightly affect contributions of iridium *d*-orbitals and π-orbitals of the ligands to the HOMO. The largest stabilization of the HOMO calculated for complex **3** can be explained by the electron-withdrawing properties of 4,4'-dicarboxy-2,2'-bipyridine which are the most pronounced among ancillary ligands studied in this work. The ancillary ligands make dominant contribution (>80%) to the lowest unoccupied molecular orbital (LUMO) of the complexes and, hence, its energy is more sensitive to the variation of the substituents. Electron-donating methyl-groups induce destabilization of the LUMO while carboxy-groups exhibit an opposite effect.

Time-dependent DFT (TDDFT) calculations helped us to gain more insights into the electronic structure of complexes **1**–**6**. Calculated electronic spectra are in good agreement with experimental UV-Vis spectra of **1**–**6** (Fig. S16). The HOMO → LUMO transitions being highly sensitive to the substituents in the ancillary ligand correspond to the charge transfer from the metal and cyclometalated ligands to the acceptor part of the complexes. However, these transitions possess very low oscillator strengths (<0.001, Table S4) and, hence, do not appear in experimental UV-Vis spectra.

Much more intensive absorption bands originate from electronic transitions from low lying molecular orbitals (HOMO-1, HOMO-2, etc.) to the LUMO, LUMO + 1 and LUMO + 2. Most of these transitions have desired directions from iridium or cyclometalated ligands to the ancillary ligand, but some intensive bands are completely localized on 2,5-diphenyloxa-

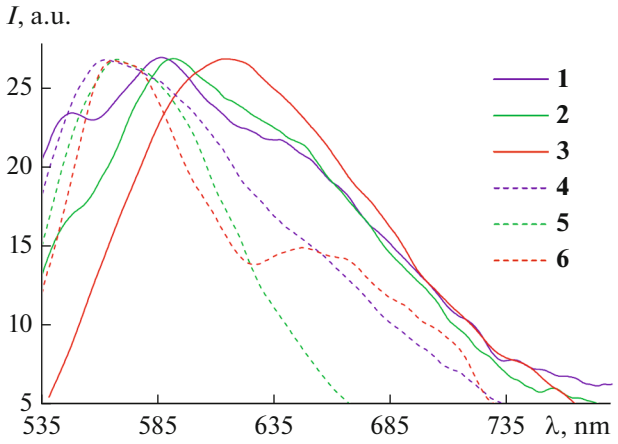

Fig. 5. Emission spectra of **1**–**6** recorded in CH_2Cl_2 at 25°C (λ_{ex} = 513 nm).

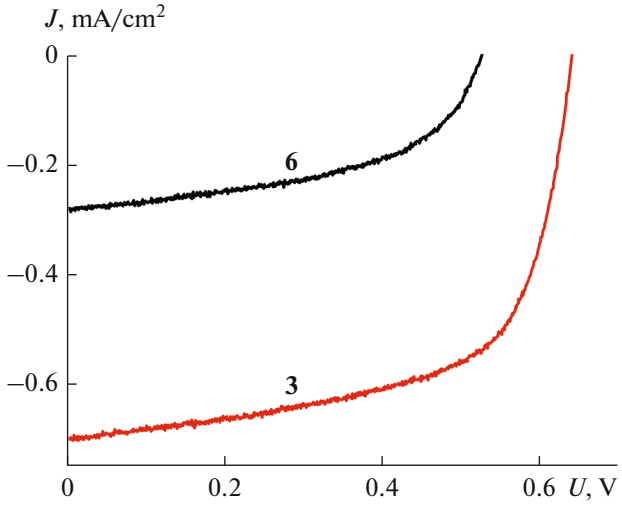

Fig. 6. Current–voltage characteristics of TiO_2 photoanodes sensitized by complexes **3** and **6** under AM 1.5 G simulated solar light (100 mW cm^{-2}) in acetonitrile solution of 0.5 M LiI + 0.05 M I_2.

zole and, hence, less suitable for photosensitization of titanium dioxide in DSSC.

Photovoltaics

The ground state oxidation potentials of **1**–**6** are all higher than 1.5 V vs. NHE (Table 1) that is sufficient to produce the driving force for the reduction of a dye by the I_3^-/I^- redox mediator. In turn, the excited state redox potentials of **1**–**6** are all smaller than –0.5 V vs. NHE (Fermi level of TiO_2), so the complexes can spontaneously inject electrons into the conduction band of the semiconductor. Two complexes bearing "anchoring" carboxy-groups (**3** and **6**) were selected and used in preparation of photoanodes for dye-sensitized solar cells.

Current density–voltage and incident photon-to-electron conversion efficiency (IPCE) curves for the prepared photoanodes are presented at Figs. 6 and 7 (see also Figs. S17, S18 for time dependence of photocurrent and photovoltage), respectively. Photoanodes based on iridium complexes demonstrate open-circuit photovoltages (V_{oc}) comparable with that of the standard ruthenium(II) dye while their short-circuit photocurrent densities (J_{sc}) are dramatically lower than that of N719 because of poor absorptivity of the iridium(III) dyes in the visible spectral range (Table 2).

Lower photocurrent density of the photoanode based on **6** may result from the nonradiative decay of the excited state of the complex (because of the extended conjugated π-system of dppz) preventing the electron injection into the conduction band of titanium dioxide. IPCE spectra match solution absorption spectra of **3** and **6** and correlate well with photovoltaic characteristics of the dyes.

Intensity modulated photocurrent and photovoltage spectra (IMPS and IMVS) of the TiO_2 photoanodes sensitized by complexes **3** and **6** are presented at Figs. S19, S20. The electron transport (τ_{tr}, time necessary for electrons to reach fluorine-tin oxide surface from the outermost photoanode surface) and electron recombination (τ_{rec}, lifetime of charge carriers) time constants were determined as follows:

$$\tau_{tr} = 1/(2\pi f_{IMPS}), \quad (1)$$

where f_{IMPS} is the frequency corresponding to the minimum of the photocurrent spectrum;

$$\tau_{rec} = 1/(2\pi f_{IMVS}), \quad (2)$$

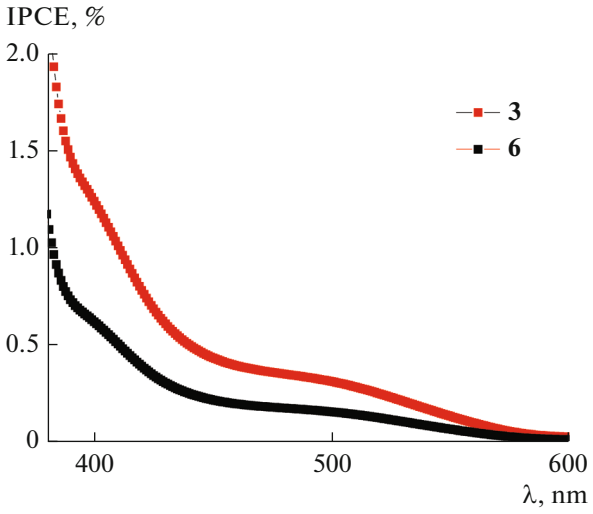

Fig. 7. Incident photon-to-electron conversion efficiency (IPCE) spectra of TiO_2 photoanodes sensitized by complexes **3** and **6** under AM 1.5 G simulated solar light (100 mW cm^{-2}).

Table 2. Photovoltaic properties of TiO_2 photoanodes sensitized by complexes **3**, **6** and **N719***

Dye	V_{oc}, V	J_{sc}, mA cm^{-2}	FF	η, %	τ_{tr}, ms	τ_{rec}, ms	h_{cc}
3	0.64	0.7	0.79	0.35	8.0	27.0	0.70
6	0.53	0.3	0.66	0.10	8.0	19.5	0.59
N719	0.75	8.2	0.80	4.92	–	–	–

* V_{oc}—open-circuit photovoltage; J_{sc}—short-circuit photocurrent density; FF—fill factor; η—power conversion efficiency; τ_{tr}—electron transport time; τ_{rec}—electron recombination time; h_{cc}—charge collection efficiency, $h_{cc} = 1-\tau_{tr}/\tau_{rec}$.

where f_{IMVS} is the frequency corresponding to the minimum of the photopotential spectrum.

The IMPS and IMVS measurements show that the lifetime of charge carriers is ~3.5 times longer than the injection time for complex **3** and is ~2.5 times longer for complex **6** which, in combination with the higher charge collection efficiency for **3**, indicate that the dicarboxybipyridine-based complex **3** is more efficient as the photosensitizer in DSSC.

CONCLUSIONS

A series of iridium(III) complexes with cyclometalated 2,5-diphenyloxazole and various ancillary ligands based on 2,2'-bipyridine or dipyridophenazine were prepared and thoroughly characterized. Crystallization of the complexes with iodine species gave interesting salts containing infinite polyiodide chains forming intermolecular contacts with the π-system of the ligands. Varying the substituents in the ancillary ligand as well as the change of its type affected optical properties of the complexes while their redox potentials related to the $Ir^{3+} \rightleftharpoons Ir^{4+}$ process were invariant to these changes. Complexes bearing "anchoring" COOH-groups successfully sensitized mesoscopic titanium dioxide but the one with 4,4-dicarboxy-2,2-bipyridine demonstrated better photovoltaic characteristics than those of its dipyridophenazine analogue.

EXPERIMENTAL

Materials and Methods

All commercially available reagents were at least reagent grade and used without further purification. Solvents were distilled and dried according to standard procedures. 2,5-Diphenyloxazole-based dimer, $[Ir(ppo)_2Cl_2]$, was synthesized according to published procedure [51]. 2,2'-Bipyridine and dipyrido[3,2-a:2',3'-c]phenazine derivatives were prepared as previously described [17]. Preparation of the heteroleptic iridium complexes was carried out under dry argon according to literature [52].

^{1}H NMR spectra were acquired at 25°C on a Bruker Avance 400 instrument and chemical shifts were reported in ppm referenced to residual solvent signals. High resolution and accurate mass measurements were carried out using a BrukermicroTOF-Q^{TM} ESI-TOF (Electro Spray Ionization/Time of Flight) and Thermo Scientific^{TM} LTQ Orbitrap mass spectrometers. Electronic absorption spectra were measured on an OKB Spectr SF-2000 spectrophotometer. Luminescent spectra were obtained on a Perkin Elmer LS-55 spectrofluorimeter. An Econix-Expert Ltd. Ecotest-VA polarograph was used for electrochemical measurements with a glassy carbon working electrode, platinum counter electrode, and saturated Ag/AgCl reference electrode. Cyclic voltammograms were recorded in Ar-saturated acetonitrile with 0.1 M $(n\text{-}Bu_4N)ClO_4$ at a scan rate of 100 mV/s. Ferrocene was used as an internal standard.

Synthesis

Complexes **1**–**6** were obtained according to a general procedure:

Cyclometalated Ir(III) dimer $[Ir(ppo)_2Cl_2]$ (20 mg, 0.015 mmol), N^N ligand (0.03 mmol) were mixed in a mixture of CH_2Cl_2/CH_3OH (20 mL, 1/1) and refluxed for 10–12 h under argon in darkness. The deeply colored solutions (orange to red) were evaporated to dryness and redissolved in CH_3OH (with addition of a minimal amount of CH_2Cl_2 if needed). A 10-fold excess of saturated solution of NH_4PF_6 in CH_3OH was added dropwise to solutions of complexes and the resulting mixtures were kept in fridge. Precipitates formed were collected, washed by cold methanol and dried in vacuum.

(2,2'-Bipyridine)-bis-(2,5-diphenyloxazolato)iridium(III) hexafluorophosphate $[Ir(ppo)_2(bpy)][PF_6]$ (1): orange powder, yield 54%.

^{1}H NMR ($CDCl_3$, ppm): δ 6.72–6.74 (m, 4H), 7.05–7.11 (m, 4H) (m, 4H), 7.38–7.50 (m, 8H), 7.69 (m, 6H), 8.10 (d, J = 5.1 Hz, 2H), 8.19 (t, J = 7.9 Hz, 2H), 8.69 (d, J = 8.1 Hz, 2H).

HRMS (ESI) m/z: $[M]^+$ Calcd. for $C_{40}H_{28}N_4O_2Ir^+$ 789.1842; Found 789.1846.

Mp = 273°C.

(4,4'-Dimethyl-2,2'-bipyridine)-bis-(2,5-diphenyloxazolato)iridium(III) hexafluorophosphate $[Ir(ppo)_2(dmbpy)][PF_6]$ (2): orange powder, yield 66%.

^{1}H NMR ($CDCl_3$, ppm): δ 2.52 (s, 6H), 6.58 (d, J = 7.6 Hz, 2H), 6.61 (s, 2H), 6.91–6.97 (m, 4H), 7.19

(d, J = 7.4 Hz, 2H), 7.29–7.34 (m, 6H), 7.51–7.57 (m, 6H), 7.81 (d, J = 5.6 Hz, 2H), 8.29 (s, 2H).

HRMS (ESI) m/z: $[M]^+$ Calcd. for $C_{42}H_{32}N_4O_2Ir^+$ 817.2155; Found 817.2143.

Mp = 265°C.

(4,4'-Dicarboxy-2,2'-bipyridine)-bis-(2,5-diphenyloxazolato)iridium(III) hexafluorophosphate [Ir(ppo)$_2$(dcbpy)][PF$_6$] (3): orange powder, yield 77%.

^{1}H NMR ($CDCl_3$/CD_3OD 1/1 + CF_3COOH, ppm): δ 6.73 (d, J = 7.0 Hz, 2H), 6.96 (s, 2H), 7.06–7.15 (m, 4H), 7.38–7.45 (m, 6H), 7.67 (d, J = 7.1 Hz, 4H), 7.72 (d, J = 7.0 Hz, 2H), 8.12 (dd, J_1 = 5.6 Hz, J_2 = 1.5 Hz, 2H), 8.36 (d, J = 5.6 Hz, 2H), 9.12 (s, 2H).

HRMS (ESI) m/z: $[M]^+$ Calcd. for $C_{42}H_{28}N_4O_6Ir^+$ 877.1638; Found 877.1638.

Mp = 330°C (dec.).

(Dipyrido[3,2-a:2',3'-c]phenazine)-bis-(2,5-diphenyloxazolato)iridium(III) hexafluorophosphate [Ir(ppo)$_2$(dppz)][PF$_6$] (4): orange powder, yield 97%.

^{1}H NMR ($CDCl_3$, ppm): δ 6.88 (d, J = 6.9 Hz, 2H), 6.99 (s, 2H), 7.09–7.17 (m, 4H), 7.28–7.41 (m, 6H), 7.65 (d, J = 7.4 Hz, 4H), 7.73 (d, J = 7.0 Hz, 2H), 8.01–8.06 (m, 4H), 8.43–8.46 (m, 2H), 8.51 (d, J = 4.2 Hz, 2H), 9.89 (d, J = 7.9 Hz, 2H).

HRMS (ESI) m/z: $[M]^+$ Calcd. for $C_{48}H_{30}N_6O_2Ir^+$ 915.2059; Found 915.2060.

Mp = 320°C (dec.).

(11,12-Dimethyl-dipyrido[3,2-a:2',3'-c]phenazine)-bis-(2,5-diphenyloxazolato)iridium(III) hexafluorophosphate [Ir(ppo)$_2$(Me$_2$dppz)][PF$_6$] (5): orange powder, yield 82%.

^{1}H NMR ($CDCl_3$, ppm): δ 2.51 (s, 6H), 6.76 (d, J = 7.2 Hz, 4H), 6.96–7.04 (m, 4H), 7.17–7.34 (m, 4H), 7.43 (d, J = 7.9 Hz, 4H), 7.62 (d, J = 7.1 Hz, 2H), 7.88–7.93 (m, 2H), 8.05 (s, 2H), 8.34 (d, J = 5.1 Hz, 2H), 9.69 (d, J = 8.2 Hz, 4H).

HRMS (ESI) m/z: $[M]^+$ Calcd. for $C_{50}H_{34}N_6O_2Ir^+$ 943.2372; Found 943.2374.

Mp = 290°C (dec.).

(11-Carboxy-dipyrido[3,2-a:2',3'-c]phenazine)-bis-(2,5-diphenyloxazolato)iridium(III) hexafluorophosphate [Ir(ppo)$_2$(dppz-COOH)][PF$_6$] (6): orange powder, yield 68%.

^{1}H NMR ($CDCl_3$, ppm): δ 6.76 (m, 2H), 7.03–7.11 (m, 4H), 7.28 (m, 6H), 7.53 (d, J = 6.5 Hz, 4H), 7.66 (d, J = 7.3 Hz, 2H), 7.99 (m, 2H), 8.35 (d, J = 8.8 Hz, 1H), 9.00 (s, 1H), 9.76–9.81 (m, 2H).

HRMS (ESI) m/z: $[M]^+$ Calcd. for $C_{49}H_{30}N_6O_4Ir^+$ 959.1958; Found 959.1960.

Mp = 330°C (dec.).

Crystallization

The crystals of **1**–**6** were obtained by the same procedure: 0.05 mmol (approx.) of a complex was placed in a snap cap glass vial (10 mm diameter, 80 mm long) with a silicone cup and dissolved in 500 μL of CH_2Cl_2/MeOH (1/1 vol) mixture. Solution was homogenized by placing in ultrasonic-bath for 3 minutes and evaporated almost to dryness in a week at 20°C. Yellow-orange crystals were obtained in all cases, but only **1**, **2**, **5**, and **6** were suitable for single crystal X-ray analysis.

Compounds **1**, **2**, **4**, and **5** were co-crystallized with the iodide-triiodide electrolyte by the following procedure: 0.05 mmol of a complex was placed in a snap cap glass vial (10 mm diameter, 80 mm long) with a silicone cup, 300 μL of 5×10^{-3} M I_2 solution in CH_2Cl_2 and 300 μL 5×10^{-2} M LiI solution in MeOH were added. The resulting solution was homogenized by placing in ultrasonic bath for 5 minutes and evaporated through a 22 g syringe needle almost to dryness in a week at 20°C. Dark-red crystals suitable for single crystal X-ray analysis were obtained for **1** and **4**.

X-ray Crystallography

Crystallographic data were collected at 150 K on a Bruker SMART APEX II diffractometer using graphite monochromatized MoK_α radiation (λ = 0.71073 Å) using a ω-scan mode. Absorption correction based on measurements of equivalent reflections was applied [53]. The structures were solved by direct methods and refined by full matrix least-squares on F^2 with anisotropic thermal parameters for all non-hydrogen atoms. In all the structures, hydrogen atoms were placed in calculated positions and refined using a riding model. In structures **4**·I_3^-·I_2 and **5**, solvent dichloromethane and methanol molecules were not located and their contribution was suppressed by the SQUEEZE procedure [54]. CCDC 2075497–2075502 contain the supplementary crystallographic data for the structures **1**, **2**, **5**, **6**, **4**·I_3^-·I_2, **1**·I_5^-, respectively. These data can be obtained free of charge from The Cambridge Crystallographic Data Centre via www.ccdc.cam.ac.uk/data_request/cif.

Photovoltaic Measurements

Photoanodes were assembled as follows. TCO22-15 fluorinated tin oxide coated 2.9 × 2.9 cm glasses (Solaronix®, specific surface resistivity ~15 Ω/sq) were purified by aging in sulfochromic mixture followed by ultrasonication in organic solvents (isopropanol and acetone) and distilled water, and then dried at 50°C in air. Application of Ti-Nanoxide paste (D/SP, Solaronix®), comprising titania powder and α-terpineol as binding agent, was performed by the standard "doctor blade" technique using a stencil with

a 2.0 × 2.0 cm (~90 μm depth) square hole. After application of the paste raw photoanodes were dried at 50°C in air, and then calcined in a muffle furnace at 450°C for 1 hour (heating rate 3°C min^{-1}, in air). The thickness of obtained titanium dioxide film was about 15 μm, and it was determined by Alpha-Step D-100 profilometer (KLA-Tencor). Sensitization of titanium dioxide was performed by soaking of photoanodes in ~5×10^{-4} M acetonitrile solutions of dye for 24 hours. A three-electrode photoelectrochemical cell PECC-2 (Zahner) was used for the photoanode potential measurements. The photoanode served as the working electrode and a platinum wire with the surface area of 5 cm^2 was used as the auxiliary electrode, a silver wire was used as the reference electrode. The voltammetric measurements were performed with an IPC Pro MF potentiostat under AM 1.5 global one sun of illumination (100 mW cm^{-2}) provided by a solar simulator (Newport 96000) in acetonitrile solution in the presence of 0.5 M LiI + 0.05 M I_2. The illumination power at different distances was determined with a Nova apparatus (OPHIR-SPIRICON Inc.). Current-voltage characteristic of DSSCs and photocurrent density at the short-circuit voltage were performed by the two-electrode scheme. Transients of photoanode potential and photocurrent density at the short-circuit voltage were measured under irradiation and in dark condition. The photoanode area was 1.0 cm^2. The illuminated photoanode area was restricted by a mask 0.196 cm^2. The illumination was performed from the side of TiO_2 photoanode with the adsorbed dye. Measurements of IMPS and IMVS as well as IPCE spectra were performed with a ZAHNER's CIMPS-QE/IPCE workstation. The photoanode was illuminated with a tunable light source, TLS03. IMVS were taken without superposition of external polarization, i.e., under open circuit conditions. IMPS were recorded under short-circuit conditions.

Density Functional Theory Calculations

All the gas-phase calculations reported in this paper have been performed within density functional theory (DFT) [55], using the hybrid functional B3LYP [56, 57]. The standard def2-SVP basis set for light elements and Stuttgart-Dresden effective core potential (ECP) for Ir atom, as implemented in the ORCA3.0 suite of programs [58], have been used together with the RIJCOSX approximation [59]. Frequency analysis was carried out to check if optimized structures were local minima. No imaginary frequencies were found for local minima. Time-dependent DFT (TDDFT) calculations were carried out at the ground state geometries to obtain vertical excitation energies and theoretical absorption spectra. The lowest 30 singlet-singlet excitations were computed.

ACKNOWLEDGMENTS

Dr. Ivan Vatsouro is acknowledged for NMR measurements and DFT calculations. Authors are grateful to the Centre of Shared Equipment of the Kurnakov Institute of General and Inorganic Chemistry for the opportunity to use X-ray equipment. Photovoltaic studies were conducted at the Frumkin Institute of Physical Chemistry and Electrochemistry.

FUNDING

The work was supported by Russian Science Foundation (project no. 19-73-00351). Photoanodes for the measurements were made within the project no. 18-29-11037 of Russian Foundation for Basic Research.

CONFLICT OF INTEREST

The authors declare that they have no conflicts of interest.

SUPPLEMENTARY INFORMATION

The online version contains supplementary material available at https://doi.org/10.1134/S1070328422700051.

REFERENCES

1. *Iridium(III) in Optoelectronic and Photonics Applications*, Zysman-Colman, E., Ed., Chichester: Wiley, 2017. https://doi.org/10.1002/9781119007166
2. Tamayo, A.B., Garon, S., Sajoto, T., et al., *Inorg. Chem.*, 2005, vol. 44, no. 24, p. 8723. https://doi.org/10.1021/ic050970t
3. Diluzio, S., Mdluli, V., Connell, T.U., et al., *J. Am. Chem. Soc.*, 2021, vol. 143, no. 2, p. 1179. https://doi.org/10.1021/jacs.0c12290
4. Mao, H.-T., Li, G.-F., Shan, G.-G., et al., *Coord. Chem. Rev.*, 2020, vol. 413, p. 213283. https://doi.org/10.1016/j.ccr.2020.213283
5. Adeloye, A.O., *Materials* (Basel), 2019, vol. 12, no. 17, p. 2734. https://doi.org/10.3390/ma12172734
6. Zhang, C., Liu, R., Zhang, D., et al., *Adv. Funct. Mater.*, 2020, vol. 30, no. 33, p. 1907156. https://doi.org/10.1002/adfm.201907156
7. Kabir, E., Wu, Y., Sittel, S., et al., *Inorg. Chem. Front.*, 2020, vol. 7, no. 6, p. 1362. https://doi.org/10.1039/C9QI01584A
8. Baranoff, E., Yum, J.H., Graetzel, M., et al., *J. Organomet. Chem.*, 2009, vol. 694, no. 17, p. 2661. https://doi.org/10.1016/j.jorganchem.2009.02.033
9. Elgar, C.E., Otaif, H.Y., Zhang, X., et al., *Chem. - Eur. J.*, 2021, vol. 27, no. 10, p. 3427. https://doi.org/10.1002/chem.202004146
10. Gayen, P., Das, U., and Banerjee, S., *J. Phys. Chem. A*, 2020, vol. 124, no. 23, p. 4654. https://doi.org/10.1021/acs.jpca.0c03102

11. Yuan, Y.J., Zhang, J.Y., Yu, Z.T., et al., *Inorg. Chem.*, 2012, vol. 51, no. 7, p. 4123. https://doi.org/10.1021/ic202423y
12. Liu, J., Chan, A.K.W., Ng, M., et al., *Organometallics*, 2019, vol. 38, no. 19, p. 3542. https://doi.org/10.1021/acs.organomet.9b00359
13. Liu, H., Gao, H., Zhao, Y., et al., *Supramol. Chem.*, 2018, vol. 30, no. 4, p. 328. https://doi.org/10.1080/10610278.2017.1406601
14. Sinopoli, A., Wood, C.J., Gibson, E.A., et al., *Eur. J. Inorg. Chem.*, 2016, vol. 2016, no. 18, p. 2887. https://doi.org/10.1002/ejic.201600242
15. Hasan, K., Bansal, A.K., Samuel, I.D.W., et al., *Sci. Rep.*, 2015, vol. 5, p. 2015. https://doi.org/10.1038/srep12325
16. Zhu, X., Cui, P., Kilina, S., et al., *Inorg. Chem.*, 2017, vol. 56, no. 22, p. 13715. https://doi.org/10.1021/acs.inorgchem.7b01472
17. Bezzubov, S.I., Dolzhenko, V.D., and Kiselev, Y.M., *Russ. J. Inorg. Chem.*, 2014, vol. 59, no. 6, p. 571. https://doi.org/10.1134/S0036023614060047
18. Shang, X., Han, D., Liu, M., et al., *RSC Adv.*, 2017, vol. 7, no. 9, p. 5055. https://doi.org/10.1039/c6ra27631h
19. Kalle, P., Kiseleva, M.A., Tatarin, S.V., et al., *Molecules*, 2022, vol. 27, no. 10, p. 3201. https://doi.org/10.3390/molecules27103201
20. Bezzubov, S.I., Kalle, P., Bilyalova, A.A., et al., *Chem. - Eur. J.*, 2018, vol. 24, no. 49, p. 12779. https://doi.org/10.1002/chem.201801963
21. Tatarin, S.V., Kalle, P., Taydakov, I.V., et al., *Dalton Trans.*, 2021, vol. 50, no. 20, p. 6889. https://doi.org/10.1039/D1DT00820J
22. Hagfeldt, A., Boschloo, G., Sun, L., et al., *Chem. Rev.*, 2010, vol. 110, no. 11, p. 6595. https://doi.org/10.1021/cr900356p
23. Lavrova, M.A., Mishurinskiy, S.A., Smirnov, D.E., et al., *Dalton Trans.*, 2020, vol. 49, no. 46, p. 16935. https://doi.org/10.1039/d0dt03564e
24. Housecroft, C.E. and Constable, E.C., *Chem. Soc. Rev.*, 2015, vol. 44, no. 23, p. 8386. https://doi.org/10.1039/c5cs00215j
25. Hewat, T.E., Yellowlees, L.J., and Robertson, N., *Dalton Trans.*, 2014, vol. 43, no. 10, p. 4127. https://doi.org/10.1039/c3dt53334d
26. Swetha, T., Reddy, K.R., and Singh, S.P., *Chem. Rec.*, 2015, vol. 15, no. 2, p. 457. https://doi.org/10.1002/tcr.201402044
27. Baranoff, E., Yum, J.H., Jung, I., et al., *Chem. – Asian J.*, 2010, vol. 5, no. 3, p. 496. https://doi.org/10.1002/asia.200900429
28. Legalite, F., Escudero, D., Pellegrin, Y., et al., *Dyes Pigm.*, 2019, vol. 171, p. 107693. https://doi.org/10.1016/j.dyepig.2019.107693
29. Bezzubov, S.I., Kiselev, Y.M., Churakov, A.V., et al., *Eur. J. Inorg. Chem.*, 2016, vol. 2016, no. 3, p. 347. https://doi.org/10.1002/ejic.201501068
30. Bezzubov, S.I., Zharinova, I.S., Khusyainova, A.A., et al., *Eur. J. Inorg. Chem.*, 2020, vol. 2020, no. 34, p. 3277. https://doi.org/10.1002/ejic.202000372
31. Bezzubov, S., Ermolov, K., Gorbunov, A., et al., *Dalton Trans.*, 2021, vol. 50, no. 45, p. 16765. https://doi.org/10.1039/D1DT03579G
32. Pashaei, B., Shahroosvand, H., Graetzel, M., et al., *Chem. Rev.*, 2016, vol. 116, no. 16, p. 9485. https://doi.org/10.1021/acs.chemrev.5b00621
33. Teuscher, J., Marchioro, A., Andres, J., et al., *J. Phys. Chem.*, 2014, vol. 118, no. 30, p. 17108. https://doi.org/10.1021/jp501481c
34. Saygili, Y., Stojanovic, M., Flores-Diaz, N., et al., *Inorganics*, 2019, vol. 7, no. 3, p. 30. https://doi.org/10.3390/inorganics7030030
35. Cong, J., Hao, Y., Sun, L., et al., *Adv. Energy Mater.*, 2014, vol. 4, no. 8, p. 1. https://doi.org/10.1002/aenm.201301273
36. Moser, J., Zakeeruddin, S.M., Nazeeruddin, M.K., et al., *J. Phys. Chem. B*, 2001, vol. 105, p. 10461. https://doi.org/10.1021/jp012075a
37. Richards, C.E., Anderson, A.Y., Martiniani, S., et al., *J. Phys. Chem. Lett.*, 2012, vol. 3, no. 15, p. 1980. https://doi.org/10.1021/jz3006755
38. Rowley, J.G., Farnum, B.H., Ardo, S., et al., *J. Phys. Chem. Lett.*, 2010, vol. 1, no. 20, p. 3132. https://doi.org/10.1021/jz101311d
39. El-Zohry, A.M. and Zietz, B., *J. Phys. Chem. C*, 2020, vol. 124, no. 30, p. 16300. https://doi.org/10.1021/acs.jpcc.0c03436
40. Tuikka, M., Hirva, P., Rissanen, K., et al., *Chem. Commun.*, 2011, vol. 47, no. 15, p. 4499. https://doi.org/10.1039/c1cc10491h
41. Madhu, S., Evans, H.A., Doan-Nguyen, V.V.T., et al., *Angew. Chem., Int. Ed.*, 2016, vol. 55, no. 28, p. 8032. https://doi.org/10.1002/anie.201601585
42. Starikov, E.B., *Int. J. Quantum Chem.*, 1997, vol. 64, no. 4, p. 473.
43. Lamberts, K., Handels, P., Englert, U., et al., *CrystEngComm*, 2016, vol. 18, no. 21, p. 3832. https://doi.org/10.1039/C6CE00396F
44. Bartashevich, E.V., Yushina, I.D., Stash, A.I., et al., *Cryst. Growth Des.*, 2014, vol. 14, no. 11, p. 5674. https://doi.org/10.1021/cg500958q
45. Wang, H., Zhang, X., Gong, F., et al., *Adv. Mater.*, 2012, vol. 24, no. 1, p. 121. https://doi.org/10.1002/adma.201103785
46. Wang, H., Liu, X., Wang, Z., et al., *J. Phys. Chem. B*, vol. 110, no. 12, p. 5970. https://doi.org/10.1021/jp057121b
47. Yanagida, S., Yu, Y., and Manseki, K., 2009. https://doi.org/10.1021/ar900069p
48. Mao, Z., Ye, Y., Lv, H., et al., *Angew. Chem., Int. Ed.*, 2020, vol. 59, no. 27, p. 10780. https://doi.org/10.1002/anie.201915824
49. Svendsen, H., Overgaard, J., Chen, Y.-S., et al., *Chem. Commun.*, 2011, vol. 47, no. 33, p. 9486. https://doi.org/10.1039/c1cc12626a
50. Tanaka, E. and Robertson, N., *J. Mater. Chem. A*, 2020, vol. 8, no. 38, p. 19991. https://doi.org/10.1039/d0ta07377f
51. Krisyuk, V.V., Turgambaeva, A.E., Lee, J., et al., *Transit. Met. Chem.*, 2005, vol. 30, no. 7, p. 786. https://doi.org/10.1007/s11243-005-5274-x

52. Bezzubov, S.I., Bilyalova, A.A., Kuznetsova, I.V., et al., *Russ. J. Inorg. Chem.*, 2017, vol. 62, no. 8, p. 1085. https://doi.org/10.1134/S0036023617080046

53. Sheldrick, G.M., *Acta Crystallogr. Sect. A: Found. Crystallogr.*, 2008, vol. 64, no. 1, p. 112. https://doi.org/10.1107/S0108767307043930

54. Spek, A.L., *J. Appl. Crystallogr.*, 2003, vol. 36, no. 1, p. 7. https://doi.org/10.1107/S0021889802022112

55. Kohn, W., Becke, A.D., and Parr, R.G., *J. Phys. Chem.*, 1996, vol. 100, no. 31, p. 12974. https://doi.org/10.1021/jp960669l

56. Becke, A.D., *Phys. Rev. A: At., Mol. Opt. Phys.*, 1988, vol. 38, no. 6, p. 3098. https://doi.org/10.1103/PhysRevA.38.3098

57. Neese, F., Wennmohs, F., Hansen, A., et al., *Chem. Phys.*, 2009, vol. 356, nos. 1–3, p. 98. https://doi.org/10.1016/j.chemphys.2008.10.036

58. Weigend, F. and Ahlrichs, R., *Phys. Chem. Chem. Phys.*, 2005, vol. 7, no. 18, p. 3297. https://doi.org/10.1039/b508541a

59. Neese, F., *WIREs Comput. Mol. Sci.*, 2012, vol. 2, no. 1, p. 73.